Electron-positron plasma drop formed by ultra-intense laser pulses

Inga Kuznetsova and Johann Rafelski

Department of Physics, The University of Arizona, Tucson, Arizona, 85721, USA

We study the initial properties and positron annihilation within a small electron-positron plasma drop formed by intense laser pulse energy. Such QED cascade generated plasma is, in general, far below the chemical (particle yield) equilibrium. We find that the available electrons and positrons equilibrate kinetically, yet despite relatively high particle density, the electron-positron annihilation is very slow, suggesting a rather long life span of the plasma drop.

I. INTRODUCTION

Conversion of the high intensity laser pulse energy into a dense gas of e^+, e^- electron-positron pairs is a topic of current theoretical and, soon, experimental interest. A QED cascade mechanism producing a rapid conversion of laser pulse energy into pairs was demonstrated in [1] for pulse intensity on the order of 10^{24} W/cm^2. Considering the known reaction cross sections [2], subsequent to the electromagnetic cascade process discussed in Ref. [1], photons escape the small plasma drop, while as we show here, the electromagnetic scattering thermalizes the momentum distribution of this relatively dense electron-positron phase. We thus find a drop of "thermal" momentum equilibrated, but "chemical" yield nonequilibrated electron-positron plasma with a size as small as a few μm and an energy content up to a kJ. Such plasma will expand and lose energy by positron annihilation. We obtain here the rates of energy and particle loss by annihilation.

The corresponding initial local energy density is provided by the laser field. We assume the formation of the plasma drop at rest in the lab frame e.g. invoking symmetric laser pulse collisions triggering QED cascades. The experimental pulse intensity parameter, defining plasma drop properties, is [3]

$$a_0 = \frac{eE_0\lambda}{m}, \qquad (1)$$

where e is the electron charge, E_0 is the laser field strength in the focus, λ is the wavelength, and m is the electron (positron) mass. The discussion of physical properties that we present corresponds to $a_0 \simeq 4000$. This value will be within the range of the next generation ultra intense pulsed lasers. For a plasma drop radius $R = 3$ μm, $2R = 3\lambda$, the corresponding total plasma drop energy is $\mathcal{O}(0.3)$ kJ.

In the present context of plasma cooling we extended the results of Ref. [2] to the lower density and lower temperature domain. The important theoretical refinement discussed here for the first time, in the context of laser generated low density e^-e^+ plasma, is the consideration of the plasmon screening depending on plasma temperature and density. We also extend our earlier considerations

to the nonrelativistic regime $T \leq m$ as required in the study of the plasma expansion and freeze-out process.

Under the experimental conditions we consider here, all photons produced will escape from the small drop of low density plasma of electrons and positrons without much, if any, scattering. However, even far from the chemical equilibrium density of the particle pair yield, it is possible for the produced electrons and positrons to equilibrate thermally by means of Møller and Bhabha scattering,

$$e^\pm + e^\pm \leftrightarrow e^\pm + e^\pm, \qquad (2)$$

$$e^\pm + e^\mp \leftrightarrow e^\pm + e^\mp, \qquad (3)$$

forming an electron-positron plasma drop: When the drop size R exceeds the scattering length L_{ee},

$$R > L_{\mathrm{ee}}, \qquad (4)$$

multiple scattering processes can occur, allowing kinetic "thermal" equilibration. We therefore study positron annihilation loss processes assuming the Fermi-Boltzmann energy distribution of available particles. We solve kinetic population equations and evaluate the fraction of particles in plasma which can annihilate during the plasma life span.

There are two paths to positron annihilation, the direct in-flight pair annihilation,

$$e^\pm + e^\mp \longrightarrow \gamma + \gamma, \qquad (5)$$

and in-flight bound state positronium p$_s$ formation,

$$e^\pm + e^\mp \rightarrow \gamma + \mathrm{Pn} \quad \mathrm{Pn} \rightarrow n\gamma, \quad n = 2, 3, \qquad (6)$$

which is followed ultimately by annihilation. The annihilation life span of positronium for spin 0 is $\tau_{\mathrm{P2}} = 0.12$ ns, while for spin 1 it is $\tau_{\mathrm{P3}} = 140$ ns. However, the positronium formation cross section only competes with the in-flight annihilation cross section for temperatures below $T \approx 60$ eV [4], and at that point, the expansion dilution will, in general, slow these processes down considerably.

In Sec. II we present cross sections for Møller and Bhabha scattering, including in the plasmon screening effects. We compare the resulting pair annihilation cross section with positronium formation. In Sec. III we present

numerical results for the Møller and Bhabha scattering mean free path and also annihilation relaxation time. We discuss conditions for the plasma drop to be thermally equilibrated. In Sec. IV we evaluate our results and present conclusions.

II. e^+, e^- PLASMA REACTION RATES

A. Scattering rates

1. Particle density

We consider the case of a small nonopaque expanding electron-positron plasma drop. The drop stays thermally equilibrated by scattering processes. The electron (positron) multiplicity N_i ($i = e^+$, e^-) is thus in thermal (momentum distribution) but not in chemical (yield distribution) equilibrium.

It has been shown [5] that in order to maximize the entropy at fixed particle number, the appropriate maximum entropy distribution is the usual Fermi-Dirac $f_{e,\bar{e}}$ distribution accompanied by a phase space occupancy parameter Υ,

$$f_{e,\bar{e}} = \frac{1}{\Upsilon^{-1} e^{(u \cdot p \mp \nu)/T} + 1}. \tag{7}$$

$\Upsilon(t)$ describes the pair density and is, in general, a function of time, and it is the same for both particles and antiparticles. This is in distinction from the behavior of the chemical potential ν which changes sign, $\nu_{\bar{e}} = -\nu_e$, comparing particles and antiparticles. The chemical potential ν regulates the abundance difference between particles and antiparticles and thus, in general, is only weakly dependent on time. A system with $\Upsilon = 1$ for all particles is in chemical equilibrium, and we refer to particle density with $\Upsilon = 1$ as a chemical equilibrium density.

Note that the Lorentz-invariant exponents involve the scalar product of the particle four-momentum p_i^{μ} with the local four-vector of velocity u^{μ}, where u^{μ} describes the local collective flow of matter, as expected for an unconfined plasma drop. The thermal properties ν, T, Υ are defined in the local rest frame. In the absence of local matter flow the local rest frame is the laboratory frame,

$$u^{\mu} = (1, \vec{0}), \qquad p^{\mu} = (E, \vec{p}). \tag{8}$$

We thus have

$$f_{e,\bar{e}} = \frac{1}{\Upsilon_{e,\bar{e}}^{-1} e^{E/T} + 1}, \qquad \Upsilon_{e,\bar{e}} = \Upsilon e^{\pm \nu/T}. \tag{9}$$

The yields of particles are

$$N_{e,\bar{e}} = n_{e,\bar{e}} V = g_{e,\bar{e}} V \int \frac{d^3 p}{(2\pi)^3} f_{e,\bar{e}}, \tag{10}$$

where $V = 4\pi R^3/3$ is the volume and $g_{e,\bar{e}} = 2$ is the spin degeneracy. When the e, $\bar{e}$-pair yield is far below chemical

equilibrium, that is, $\Upsilon \ll 1$, the effects of quantum statistics are, in general, less significant, and the Boltzmann limit is often equally precise,

$$f_{e,\bar{e}} \rightarrow \Upsilon_{e,\bar{e}} e^{-E/T}. \tag{11}$$

2. Plasmon mass and screening length

To avoid Coulomb singularity in reaction matrix elements we introduce the plasmon mass, induced by the plasma screening effect, following the example of gluon dynamics in quark-gluon plasma [6]. The plasmon mass is [7]

$$m_{\gamma}^2 = \omega_{\mathrm{pl}}^2 = 8\pi\alpha \int \frac{f_{e^+} + f_{e^-}}{E_e}\left(1 - \frac{p^2}{3E_e^2}\right)\frac{dp^3}{(2\pi)^3}. \tag{12}$$

$\alpha = e^2/4\pi = 1/137.036$ is the fine-structure constant. For nonrelativistic temperatures $T \ll m_e$, m_{γ} goes to the classical plasma frequency, and a simple limit also emerges for relativistic temperatures with $\Upsilon = 1$,

$$m_{\gamma} \approx \begin{cases} 4\pi\sqrt{2\alpha n_e/m_e}, & T < m_e, \\ \sqrt{4\pi\alpha}T/3, & T > m_e, \Upsilon = 1. \end{cases} \tag{13}$$

The corresponding screening length, the Debye radius, is

$$r_D = \frac{v_T}{\omega_{\mathrm{pl}}}, \tag{14}$$

and the mean thermal particle velocity v_T is

$$v_T = \frac{\int \frac{p}{E} f d^3 p}{\int f d^3 p} \tag{15}$$

since $f_{e^+} = f_{e^-} = f$. We show in Fig. 1 the electron (positron) screening length and the mass of the plasmon as a function of T. The plasmon mass is increasing towards the small temperatures and is asymptotically constant, similar to the behavior of the plasma density. The screening length is otherwise decreasing towards the small temperatures (inverse proportional to m_{γ} and $v_T \propto \sqrt{T}$) in our range of temperature.

3. Boltzmann limit

We are interested in the experimental conditions under which the number of pairs produced is large compared to the residual electron density originating in matter. Furthermore, we will deal with conditions ($\Upsilon_e < 1$ or/and $T \leq m$ MeV) which allow us to use the Boltzmann approximation. Then, we have

$$\frac{n_e - n_{\bar{e}}}{n_e + n_{\bar{e}}} \rightarrow \sinh(\nu/T) \ll 1. \tag{16}$$

In what follows, we will set $\nu = 0$, and consider elsewhere the case for very low density degenerate plasma, where the chemical potential may become important. We thus have
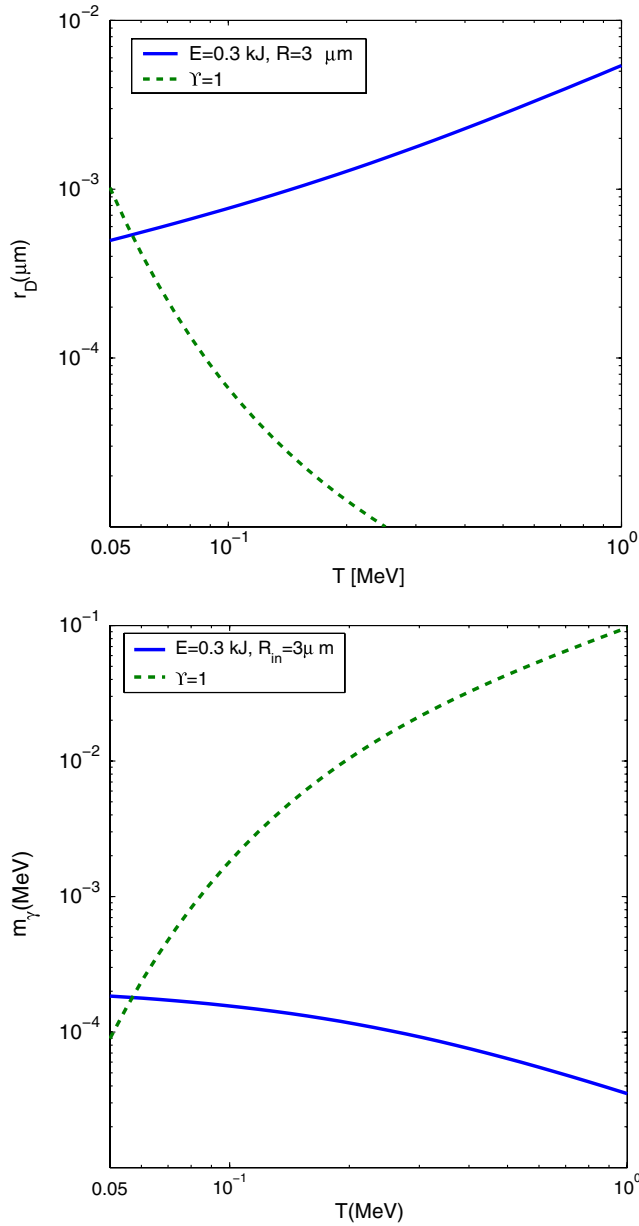
FIG. 1 (color online). Upper panel: electron (positron) screening length as a function of plasma temperature. Lower panel: mass of the plasmon as a function of T.

$\Upsilon_{e,\bar{e}} = \Upsilon$. In the relativistic Boltzmann (classical) limit the plasma density and energy density are

$$n_e = \frac{\Upsilon_e g_e T^3}{2\pi^2} x^2 K_2(x),$$

(17)

$$\epsilon = \Upsilon_e \frac{3 g_e T^4}{2\pi^2}\left(x^2 K_2(x) + \frac{1}{3} x^3 K_1(x)\right),$$

(18)

where $K_i(x)$ is a Bessel function, $x = m/T$.

4. Electron (positron) scattering rates

In the evaluation of the matrix element we use Mandelstam variables: s, u, and t. In the case of Møller scattering

$$s = (p_1 + p_2)^2, \qquad u = (p_3 - p_2)^2,$$
$$t = (p_3 - p_1)^2,$$

(19)

and $s + u + t = m_1^2 + m_2^2 + m_3^2 + m_4^2$.

The Møller scattering matrix element is [2,8,9]

$$|M_{e^\pm e^\pm}|^2 = 2^6 \pi^2 \alpha^2 \left\{ \frac{s^2 + u^2 + 8m^2(t - m^2)}{2(t - m_\gamma^2)^2} \right.$$
$$+ \frac{s^2 + t^2 + 8m^2(u - m^2)}{2(u - m_\gamma^2)^2}$$
$$\left. + \frac{(s - 2m^2)(s - 6m^2)}{(t - m_\gamma^2)(u - m_\gamma^2)} \right\}.$$

(20)

In the case of Bhabha scattering we have

$$s = (p_3 - p_2)^2, \qquad u = (p_1 + p_2)^2,$$
$$t = (p_3 - p_1)^2;$$

(21)

see diagrams in [2]. The matrix element does not change in terms of variables p_1, p_2, p_3; when written in terms of variables s, u, t we need to cross u and s in the Møller scattering matrix element [see Eq. (20)],

$$|M_{e^\pm e^\mp}(s, t, u)|^2 = |M_{e^\pm e^\pm}(u, t, s)|^2;$$

(22)

thus we find

$$|M_{e^\pm e^\mp}|^2 = 2^6 \pi^2 \alpha^2 \left\{ \frac{s^2 + u^2 + 8m^2(t - m^2)}{2(t - m_\gamma^2)^2} \right.$$
$$+ \frac{u^2 + t^2 + 8m^2(s - m^2)}{2(s - m_\gamma^2)^2}$$
$$\left. + \frac{(u - 2m^2)(u - 6m^2)}{(t - m_\gamma^2)(s - m_\gamma^2)} \right\}.$$

(23)

For Møller and Bhabha scattering the cross section $\sigma_{ee}(s)$ can be obtained by averaging the matrix element over the t variable:

$$\sigma_{ee}(s) = \frac{1}{16\pi(s - 4m^2)^2} \int_{t_{\min}}^{t_{\max}} dt |M_{ee}|^2,$$

(24)

where $t_{\min} = -(s - 4m^2)$, $t_{\max} = 0$ in both cases [2]. Similar evaluations were done for heavy quark production [10].

For Møller and Bhabha cross sections we obtain in plasma, keeping m_γ,

$$\sigma_{e^{\pm}e^{\pm}\leftrightarrow e^{\pm}e^{\pm}}(s) = \frac{1}{16\pi(s-4m^2)^2}\int_{-(s-4m^2)}^0 dt |M_{e^{\pm}e^{\pm}}|^2$$

$$= \frac{4\pi\alpha^2}{(s-4m^2)}\left(\frac{s^2+8m^2(m_\gamma^2-m^2)+(s+m_\gamma^2-4m^2)^2}{(s+m_\gamma^2-4m^2)m_\gamma^2}+1\right)+\frac{8\pi\alpha^2}{(s-4m^2)^2}\left(\frac{(s-2m^2)(s-6m^2)}{(s-4m^2+2m_\gamma^2)}+s+m_\gamma^2\right)$$

$$\times \ln\frac{m_\gamma^2}{s-4m^2+m_\gamma^2}; \tag{25}$$

$$\sigma_{e^{\pm}e^{\mp}\leftrightarrow e^{\pm}e^{\mp}}(s) = \frac{1}{16\pi(s-4m^2)^2}\int_{-(s-4m^2)}^0 dt |M_{e^{\pm}e^{\mp}}|^2$$

$$= \frac{2\pi\alpha^2}{(s-4m^2)}\left[\frac{s^2+8m^2(m_\gamma^2-m^2)+(s+m_\gamma^2-4m^2)^2}{(s+m_\gamma^2-4m^2)m_\gamma^2}+1+\frac{8((s-4m^2)^2+m^2(s-m^2))}{3(s-m_\gamma^2)^2}\right.$$

$$\left.+\frac{3s+2m_\gamma^2+4m^2}{(s-m_\gamma^2)}+2\frac{(m_\gamma^2+s)^2-4m^4+(s^2-m_\gamma^4)}{(s-m_\gamma^2)}\ln\frac{m_\gamma^2}{s-4m^2+m_\gamma^2}\right]. \tag{26}$$

B. $e + \bar{e}$ annihilation

1. Master equation and annihilation time constant

The master population equation reads

$$\frac{1}{V}\frac{dN_{e,\bar{e}}}{dt} = -\Upsilon_e\Upsilon_{\bar{e}}W_{\text{ann}}. \tag{27}$$

We have made explicit the dependence of the evolution of the particle (pair) multiplicity in thin plasma on the prevailing density showing the factor $\Upsilon_e\Upsilon_{\bar{e}}$.

A simplified form of the master equation (up to dilution by volume expansion, to be considered elsewhere) is easily obtained,

$$\frac{1}{\Upsilon_e}\frac{d\Upsilon_e}{dt} = -\frac{1}{\tau_{\text{ann}}^e}\frac{\Upsilon_{\bar{e}}}{\Upsilon_{\bar{e}}^{\text{in}}}, \tag{28}$$

introducing the annihilation relaxation time τ_{ann}^e [2],

$$\tau_{\text{ann}}^e = \frac{dn_e/d\Upsilon_e}{\Upsilon_e^{\text{in}}W_{\text{ann}}}, \tag{29}$$

and similarly for $\tau_{\text{ann}}^{\bar{e}}$. In our case $\Upsilon_e \simeq \Upsilon_{\bar{e}}$ and we see that

$$\frac{\Upsilon_{\bar{e}}^{\text{in}}}{\Upsilon_{\bar{e}}} = \int_0^t \frac{dt'}{\tau_{\text{ann}}^{\bar{e}}}(t'). \tag{30}$$

We can write a similar master equation for the plasma drop energy loss,

$$\frac{1}{V}\frac{dE^{\text{tot}}}{dt} = -\Upsilon_e\Upsilon_{\bar{e}}W_{\text{ann}}^E, \tag{31}$$

where E^{tot} is the total energy of the plasma drop. The relaxation time of energy loss is

$$\tau_{\text{ann}}^E = \frac{d\epsilon/d\Upsilon_e}{\Upsilon_e^{\text{in}}W_{\text{ann}}^E}, \tag{32}$$

where ϵ is the plasma energy density and Υ_e^{in} is the initial electron (positron) phase space occupancy.

2. Annihilation rate in flight

When electrons collide with positrons, they can annihilate. We consider here the dominant in-flight annihilation process into two photons. The invariant rate of annihilation per unit of volume and time $e + \bar{e} \to \gamma + \gamma$ is $(3 + 4 \to 1 + 2)$

$$W_{\text{ann}} = \frac{g_e^2}{2(2\pi)^8}\int\frac{d^3p_1^\gamma}{2E_1^\gamma}\int\frac{d^3p_2^\gamma}{2E_2^\gamma}\int\frac{d^3p_3^e}{2E_3^e}\int\frac{d^3p_4^{\bar{e}}}{2E_4^{\bar{e}}}\delta^4(p_1^\gamma+p_2^\gamma-p_3^e-p_4^{\bar{e}})$$

$$\times \sum_{\text{spin}}|\langle p_1^\gamma p_2^\gamma|M_{\gamma\gamma\leftrightarrow e\bar{e}}|p_3^e p_4^{\bar{e}}\rangle|^2 e^{u\cdot(p_1^e+p_2^e)/T}f_e(p_3^e)\Upsilon_e^{-1}f_{\bar{e}}(p_4^{\bar{e}})\Upsilon_{\bar{e}}^{-1}. \tag{33}$$

Here $\langle p_1^\gamma p_2^\gamma|M_{\gamma\gamma\leftrightarrow e\bar{e}}|p_3^e p_4^{\bar{e}}\rangle$ is the annihilation quantum matrix element which we will consider to lowest order in α, where g_e is the electron-positron degeneracy, and the factor $1/2$ is due to the indistinguishability of the final state photons. We used this method to describe the electron-positron pair annihilation in [2], adapting it from work on strangeness production in quark-gluon plasma [11–14]. In the last line of Eq. (33) we introduce $\Upsilon_e^{-1}\Upsilon_{\bar{e}}^{-1}$ to compensate for the factor $\Upsilon_e\Upsilon_{\bar{e}}$ seen in Eq. (27).

The invariant rate Eq. (33) relates to the electron-positron pair annihilation cross section [15]; in the Boltzmann limit we have

$$W_{\text{ann}} = \frac{g^2T}{32\pi^4}\int_{4m^2}^\infty ds\sqrt{s}(s-4m^2)\sigma_{ee\to\gamma\gamma}(s)K_1(\sqrt{s}/T). \tag{34}$$

Here the annihilation cross section is [2]

$$\sigma_{ee\to\gamma\gamma}(s) = \frac{2\pi\alpha^2(s^2 + 4m^2s - 8m^4)}{s^2(s - 4m^2)}$$

$$\times\left(\ln\frac{\sqrt{s} + \sqrt{s - 4m^2}}{\sqrt{s} - \sqrt{s - 4m^2}}\right.$$

$$\left.-\frac{(s + 4m^2)\sqrt{s^2 - 4m^2s}}{(s^2 + 4m^2s - 8m^4)}\right). \qquad (35)$$

3. Energy loss

Once in-flight $e + \bar{e}$ annihilation occurs, the produced photons escape the small plasma volume. An analogous expression to Eq. (33) describes the energy loss rate due to pair annihilation,

$$W^E_{\rm ann} = \frac{g^2_\gamma}{2(2\pi)^8}\int\frac{d^3p^\gamma_1}{2E^\gamma_1}\int\frac{d^3p^\gamma_2}{2E^\gamma_2}\int\frac{d^3p^e_3}{2E^e_3}$$

$$\times\int\frac{d^3p^e_4}{2E^e_4}\delta^4(p^\gamma_1 + p^\gamma_2 - p^e_3 - p^e_4)$$

$$\times\sum_{\rm spin}|\langle p^\gamma_1 p^\gamma_2|M_{ee\to\gamma\gamma}|p^e_3 p^e_4\rangle|^2$$

$$\times(E^e_3 + E^{\bar{e}}_4)f_e(p^e_3)f_{\bar{e}}(p^e_4)\Upsilon^{-2}_e e^{u\cdot(p^\gamma_1 + p^\gamma_2)/T}. \qquad (36)$$

We now obtain a relation analogous to Eq. (34). Consider the integral [15] leading to Eq. (34),

$$\int d^4 p\, e^{-\beta p\cdot u}\delta_0(p^2 - s) = \frac{2\pi}{\beta}\sqrt{s}K_1(\beta\sqrt{s}), \qquad (37)$$

where $u = (1, \vec{0})$ in the laboratory frame. Instead, we now need to use

$$\int d^4 p\, p\cdot u e^{-\beta p\cdot u}\delta_0(p^2 - s) = -\frac{\partial}{\partial\beta}\frac{2\pi}{\beta}\sqrt{s}K_1(\beta\sqrt{s}).$$

$$(38)$$

We use $d[K_1(x)/x]/dx = -K_2(x)/x$ to obtain

$$W^E_{\rm ann} = \frac{g^2 T}{32\pi^4}\int^\infty_{s_{th}} ds\, s(s - 4m^2)\sigma_{ee\to\gamma\gamma}(s)K_2(\sqrt{s}/T). \qquad (39)$$

4. Positronium formation

The cross section for radiative positronium $(e\bar{e})$ formation, $e^- + e^+ \leftrightarrow \gamma + (e\bar{e})$ [16], is

$$\sigma_{\rm pos} = \frac{2^{12}\pi^2\omega}{3pm^2}\xi\left(\frac{\xi^2}{1 + \xi^2}\right)^3\frac{e^{-4\xi\,{\rm arccot}\xi}}{1 - e^{-2\pi\xi}}\left(1 + \frac{\omega^2(1 - \xi^2)}{5p^2}\right),$$

$$(40)$$

where $\xi = \alpha m/2p$ and the photon energy ω is defined by the conservation law

$$\omega + \frac{\omega^2}{4m} = p^2/m + \alpha^2 m/4. \qquad (41)$$

p is the electron (positron) momentum in the center of mass reference frame, $p = \sqrt{s - 4m^2}/2$. Equation (40) is

valid while $\xi \leq 1$. This condition is satisfied up to temperatures on the order of 10 eV.

We did not consider in detail the influence of plasma screening on positronium formation, a topic which invites further work in view of currently available results. It was found in [17] that the plasma screening and collective effects significantly reduce the radiative recombination cross section in nonideal plasma. The screening effect for positronium formation should be similar to the results for free electron radiative recombination with ions in nonideal classical plasmas. However, in positron-hydrogen plasma the Debye screening can result in a large increase of the positronium formation cross section at incident positron energy 20–100 eV [18].

III. RESULTS FOR LASER FORMED PLASMA

A. Parameters for thermal plasma drop

We assume here that the total energy E of (colliding) laser pulses converts in the initial volume V to the e^+e^--plasma drop energy. The initial energy density $\epsilon = E/V$ is obtained from Eq. (1) and is characterized by a_0 and λ,

$$\epsilon = \frac{1}{4\pi}E^2_0 = \frac{1}{4\pi}\left(\frac{a_0 m}{e\lambda}\right)^2. \qquad (42)$$

The phase space occupancy of the plasma drop is

$$\Upsilon_e = \frac{1}{4\pi\epsilon_0(T)}\left(\frac{a_0 m}{e\lambda}\right)^2, \qquad (43)$$

where we introduced the chemical equilibrium energy density $\epsilon_0 = \epsilon|_{\Upsilon_e=1}$, Eq. (18). Then the total energy of plasma, E, is defined by the plasma drop radius R for a given parameter a_0 and wavelength λ. The initial plasma size is expected to be close to the wavelength. We take the wavelength $R = 3\lambda/2$ for all cases considered below.

In Fig. 2 we show the phase space occupancy Υ_e from Eq. (43) (upper panel) and the corresponding plasma density $n_{\rm pl}$ (lower panel). The solid (blue) line shows the actual chemical nonequilibrium value. For comparison, the chemical equilibrium results are shown by the dashed (green) line. We note that for $T \gg 0.06$ MeV the fully equilibrated yield is much greater than what we can make using a near future high intensity laser. However, the density of particles in plasma which we achieve is very high.

At $T \ll m$, when plasma becomes nonrelativistic the energy/particle $\to mc^2$ is a constant and does not depend much on the plasma temperature. Hence, the plasma particle density goes, for $T \to 0$, to a constant for a given energy and plasma drop size,

$$n_{\rm pl} = n_e + n_{\bar{e}} = \frac{\epsilon}{mc^2}, \qquad (44)$$

and the temperature cannot be determined considering the given available energy constraint.

In a system where particle (pairs) can be produced but energy is fixed, the entropy density reaches a maximum at $\Upsilon = 1$. We show the entropy density of electron-positron plasma,

$$s = \int \frac{d^3p}{2\pi^3}((f_e - 1)\ln(1 - f_e) - f_e \ln(f_e)), \quad (45)$$

at $E = 0.3$ kJ and $R = 3$ μm as a function of temperature in Fig. 3. As expected, the maximum of the entropy density
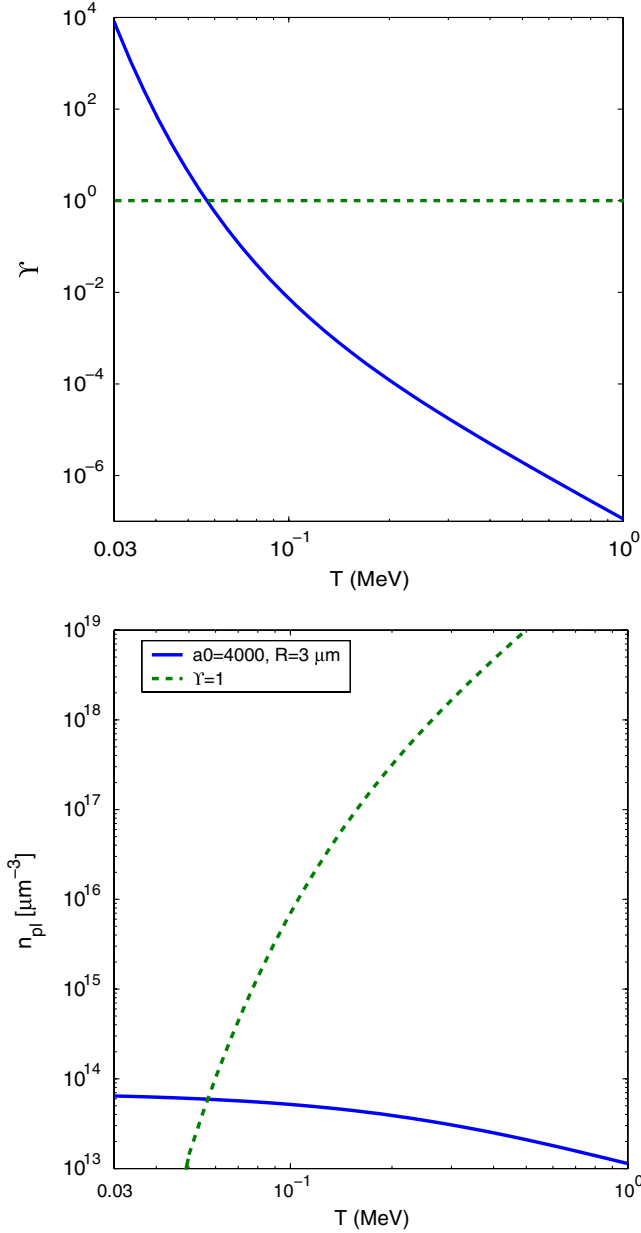
is at the temperature $T = 0.06$ MeV, where the phase space occupancy of the electron and positron $\Upsilon_e = 1$. However, the maximum is very flat. Note that there is much less entropy density when the system is formed at relatively high temperature. This is because there are fewer particle pairs and, for a relativistic gas, the entropy per particle is near $S/N \simeq 4$. For far off equilibrium low density systems the expansion of the volume is thus accompanied by reactions that tend to chemically equilibrate the system and move it towards chemical equilibrium.

B. Electron and positron scattering

The formation of electron-positron plasma is further subject to the opacity condition Eq. (4). To check if this condition is satisfied we extend our earlier considerations [2], now introducing plasmon mass, Eq. (12), in a domain of mild relativistic and nonrelativistic temperatures.

The electron (positron) mean free path follows from

$$L_{\text{ee}} = \frac{n_e}{W_{\text{ee}}}, \quad (46)$$

where for the scattering rate W_{ee} we use an equation similar to Eq. (34) (since the final state does not have two identical bosons, the normalization factor is different):

$$W_{\text{ee}} = \frac{g^2 T}{32\pi^4} \int_{4m^2}^{\infty} ds \sqrt{s}(s - 4m^2)\sigma_{\text{ee}}(s)K_1(\sqrt{s}/T) \quad (47)$$

and

$$\sigma_{\text{ee}} = \sigma_{e^+e^+ \leftrightarrow e^-e^-} + \sigma_{e^-e^+ \leftrightarrow e^+e^-}. \quad (48)$$

FIG. 2 (color online). Upper panel: electron (positron) phase space occupancy Υ_e as a function of T for $a_0 = 4000$ and $R = 3$ μm (solid blue line). Lower panel: plasma density corresponding to the phase space occupancy on the upper panel (solid blue line) and equilibrium density $\Upsilon = 1$ (dashed green line) as a function of T.

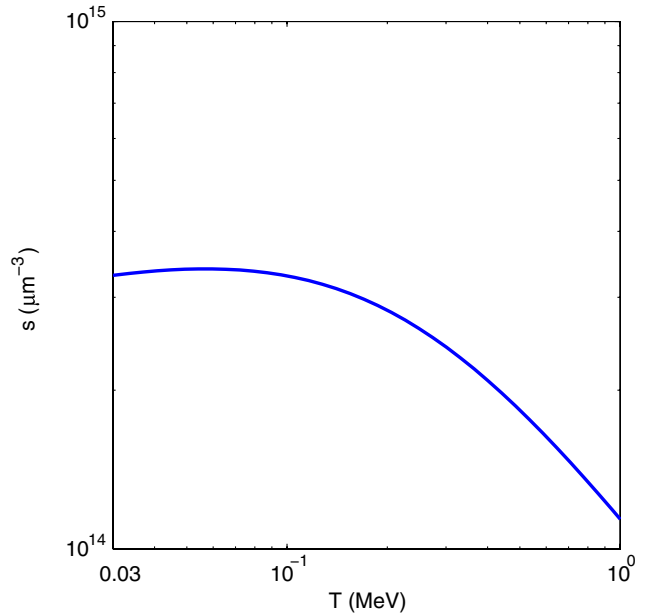FIG. 3 (color online). The entropy density of electron-positron plasma with $a_0 = 4000$ and $R = 3$ μm as a function of temperature.

In Fig. 4 we show the electron (positron) scattering length L_{ee}, Eq. (46), at a given plasma radius $R = 3$ μm and energy 0.3 kJ ($a_0 = 4000$) as a function of plasma temperature T. Υ varies for every value of T, as we see in Fig. 2. Since $\Upsilon_e \ll 1$ the scattering length can be evaluated in the Boltzmann limit in practically the entire temperature range of interest, including $T > m$. We also show (dashed green line), for comparison, the case $\Upsilon_e = 1$, which means that we allow the density to go up significantly and the small difference we see in Fig. 4 for high T is due to quantum gas properties.

At relativistic temperatures $T \simeq 1$ MeV our present result is in agreement with scattering rates evaluated with plasmon mass taken in the limit of ultrarelativistic temperatures in [2] with an accuracy of few percent.

For constant plasma drop energy the scattering length L_{ee} has a maximum at $T \approx m$. In the whole temperature range the plasmon mass is small and the first term in Eqs. (25) and (26) is dominant, resulting in the cross section for electron or positron scattering,

$$\sigma_{ee} \propto m_\gamma^{-2} \propto n_e^{-1}. \tag{49}$$

In the range where condition (49) is valid, the electron (positron) mean free path does not depend on density or Υ_e. When the mean free path is increasing with decreasing density, this is compensated by a larger cross section because of a smaller plasma screening effect or smaller m_γ. For the entire T range, the scattering length scale is a tiny fraction of the plasma size.

In the temperature range $T < m$ the contribution of $4p^2 = s - 4m^2$ is much smaller than m^2 and much larger

FIG. 4 (color online).   Electron (positron) scattering length at a given plasma radius and energy as a function of T.

than m_γ^2, and the approximate cross sections for Møller and Bhabha scatterings, Eqs. (25) and (26), are

$$\sigma_{e^\pm e^\pm \leftrightarrow e^\pm e^\pm}(s) = 2\sigma_{e^\pm e^\mp \leftrightarrow e^\pm e^\pm}(s) = \frac{64\pi\alpha^2}{(s - 4m^2)^2} \frac{m^4}{m_\gamma^2}. \tag{50}$$

One can also consider a Rutherford-type differential cross section for Møller scattering [9],

$$\frac{d\sigma}{d\cos\theta} = \frac{\pi\alpha^2 m^2}{4p^4} \csc^4\theta/2. \tag{51}$$

We checked by integrating Eq. (51) numerically that Eq. (50) corresponds to the total cross section from the integrated Eq. (51) with a cutoff angle $\theta_{\min} = m_\gamma/m$.

We found from the results presented in Fig. 4 that condition Eq. (4) is satisfied for all temperature ranges considered. We conclude that the electron-positron plasma drop can stay thermally equilibrated at relatively low densities when $\Upsilon \ll 1$ and/or the temperature $T \ll m$: the electron-positron mean free path decreases when the temperature decreases below the electron mass because of the factor $s - 4m^2 = 4p^2$ in the denominator of the cross section, Eq. (50). At a temperature higher than m the other terms begin to contribute to cross sections, Eqs. (25) and (26). The electron-positron mean free path decreases again.

The cross section, Eq. (50), is valid in the temperature range

$$T_{\mathrm{cr}} = \frac{2\pi\alpha n_e}{m^2} < T < m. \tag{52}$$

The reader should keep in mind that the present considerations do not automatically apply to the case of a degenerate electron-positron gas (high density or/and low temperature), where we should extend the investigation of collective plasmon dynamics in order to obtain a valid estimate of the electron-positron scattering cross section.

C. Annihilation

1. Plasmons

While screening and plasma oscillations impact the scattering processes, this is not the case for our domain in regard to the annihilation process. There are several processes to consider:

(1) The electron (positron) thermal mass correction, which is on the order of magnitude of m_γ. However, $m_\gamma \ll m_e$ and this correction is small.

(2) Plasmon $\leftrightarrow e^+ e^-$, when the reaction threshold is exceeded, $m_\gamma > 2m_e$ [6]. This can only happen at ultrarelativistic temperatures. In the case considered here with constant plasma energy, $m_\gamma^2 \propto T^{-1}$ (see Fig. 1), the threshold condition cannot be satisfied.

(3) The hard photons from annihilation ($k \approx m$) rescattering on plasmons. The condition where screening has a noticeable effect on the photon propagation is [19]

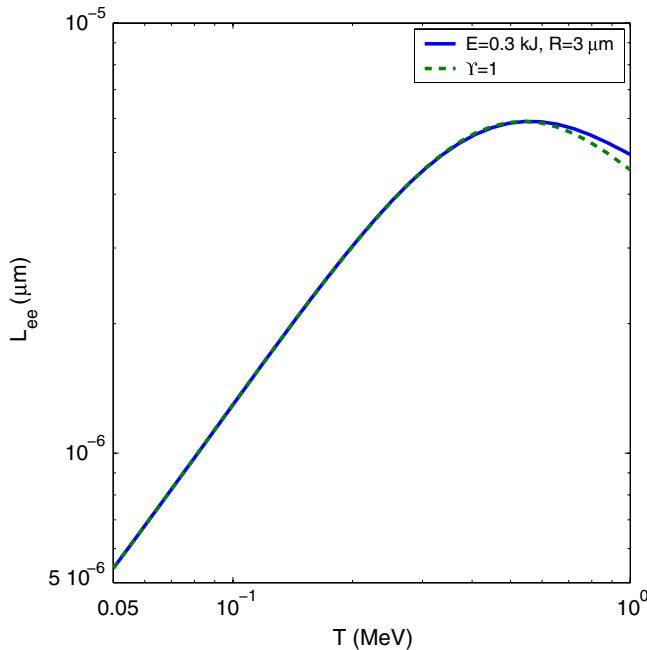$$kr_D \leq 1, \tag{53}$$

where k is the photon wave number and r_D is the Debye radius, Eq. (14). This condition is equivalent to the condition $T < T_{\mathrm{cr}}$, Eq. (52). We do not consider here such low temperature plasma.

2. Annihilation life span

We determine, using the perturbative QED reaction rate, the annihilation rate of plasma under the conditions considered in the previous subsections. We assume that the plasma drop formation life span is on the order of magnitude of the laser pulse duration, 10 fs, and this is the stage at which the density of pairs and thus annihilation should have the largest rate; however, this is not the case since, as T increases, the pair density drops, given the constant initial total energy, and thus the annihilation relaxation time increases.

In Fig. 5 we show relaxation times τ for particle number annihilation τ_{ann} (thick lines) and energy loss τ_{ann}^{E} (thin lines) for plasma at $a_0 = 4000$, $E = 0.3$ kJ (solid blue lines) and $a_0 = 8000$, $E = 1.2$ kJ (dashed green lines) as a function of temperature. The values of τ are indeed largest for initial highest temperatures, and there is a shallow minimum at $T \approx 0.065$ MeV. At $T < 0.065$ MeV the pair density is approximately constant, but the particle temperature decrease results in an increase of the annihilation relaxation time. The fastest annihilation occurs here because we have, at this low temperature, the highest mobility of particles at high density.
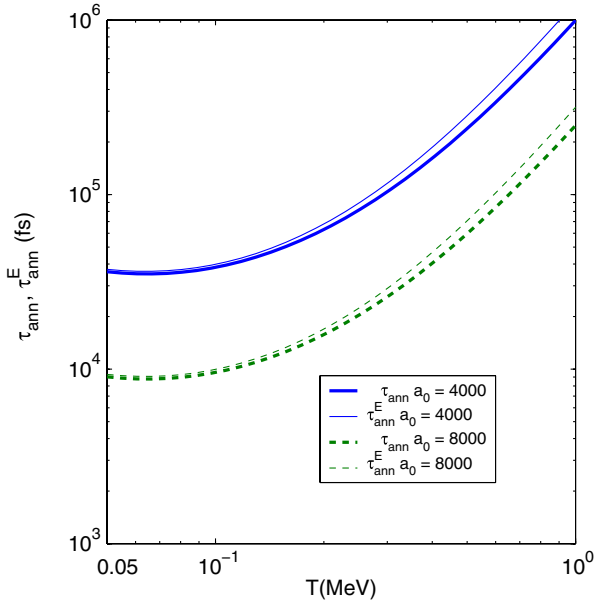

FIG. 5 (color online). Time constant for particle annihilation (thick lines) and energy loss (thin lines) at $a_0 = 4000$, $E = 0.3$ kJ (solid blue lines) and $a_0 = 8000$, $E = 1.2$ kJ (dashed green lines) as a function of plasma drop temperature.

We recognize that the fraction of annihilations is very small initially; we obtain from Eq. (27)

$$N_{\mathrm{ann}}/N_0 \approx \Upsilon_{\mathrm{e}}^2 W_{\mathrm{ann}} \frac{t}{n_0} \approx \frac{t}{\tau_{\mathrm{ann}}}. \tag{54}$$

Another way to look at the conditions for annihilation is to note that the relaxation time is inversely proportional to Υ_{e}. Then from Eq. (42) we have

$$\tau_{\mathrm{ann}} \propto \frac{\lambda^2}{a_0^2}, \tag{55}$$

which explains the dependence on a_0 (see Fig. 5).

We see in Fig. 5 that the energy loss relaxation time τ_{ann}^{E} becomes very close to τ_{ann} for $T < m$, since the energy of the plasma drop changes mostly because of the pair mass disappearance and the resulting decrease in plasma mass. At $T > 2m$, the energy loss relaxation time is, as expected, above the annihilation relaxation time. This happens since there is a preference for slower particles to annihilate, and thus on average, in the thermal bath fewer particles at higher energy are lost, and annihilation leads to a slight increase of the ambient plasma temperature.

Our result seen in Fig. 5 implies that the annihilation process, even at the highest initial density, is relatively slow compared to other dynamical effects controlling the plasma drop: the plasma drop must live $t \gg \tau_{\mathrm{ann}}$ to have most positrons in the plasma annihilated. This time is much longer than the pulse duration, 10 fs; indeed, it is on the scale of nanoseconds. There is, furthermore, the kinetic expansion leading to further dilution of the plasma—when the plasma drop expands with time, the density decreases and the annihilation relaxation becomes even longer. Most, if practically not all of the 3×10^{-4}–10^{-5} annihilation events originate in the densest plasma stage during laser pulse, and a reliable prediction of the total annihilation yield requires detailed control of the kinetic processes in the initial state of the plasma as well as a precise understanding of the plasma drop expansion dynamics, which further reduces the annihilation rate, ultimately leading to a cloud of streaming electrons and positrons.

3. In-flight annihilation compared to positronium formation

In Fig. 6 we compare the nonrelativistic limit of the annihilation in-flight cross section (dashed line) to the cross section for radiative positronium $(e\bar{e})$ formation (solid blue line) as a function of electron (positron) kinetic energy in the center of mass frame $E_{\mathrm{kin}} = (s - 4m^2)/8m$. The cross sections intersect at $E_{\mathrm{kin}} \approx 150$ eV. This corresponds to the crossover temperature obtained in [4], $T_e \simeq 60$ eV. Thus, the direct annihilation dominates down to this low temperature, and our prior results apply for $T > T_e$. For $T < T_e$ we have significant positronium formation only if we reach this condition without much expansion, which is not part of our present study.
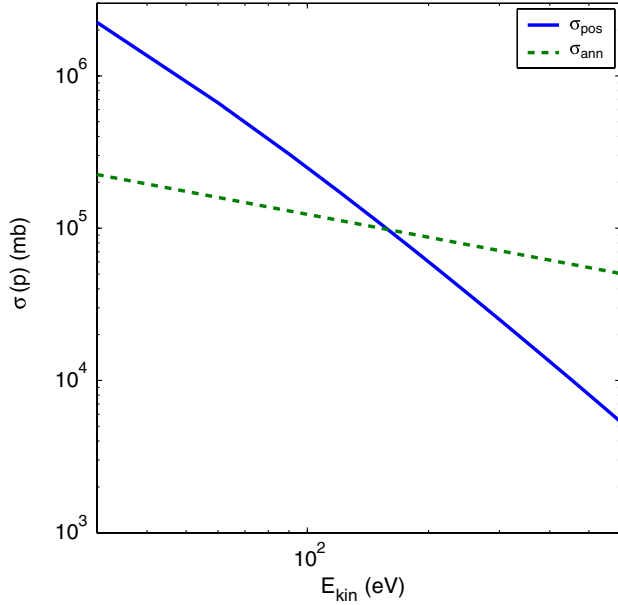
FIG. 6 (color online). Radiative positronium formation (solid line) and direct annihilation cross sections (dashed line) as functions of electron (positron) kinetic energy in the two particle center of momentum frame.

IV. CONCLUSIONS

The key result of this study is that high intensity QED cascading leads to an electron-positron drop which does not annihilate but thermally equilibrates. In this plasma drop electron-positron pairs are thermalized by Møller [Eq. (2)] and Bhabha [Eq. (3)] scattering, and they annihilate very slowly; see Fig. 5.

We found that in the Boltzmann limit the electron and positron scattering length nearly does not depend on plasma density in the considered temperature range due to collective plasmon effects. The cross section decrease at lower density is compensated by plasmon charge screening in the less dense plasma. As a result, electron-positron plasma can be thermally equilibrated at the density and temperature range considered, far below the chemical equilibrium of the pair yield, $Y = 1$. The plasma drop size allows very many scattering processes; we did not find any restriction on the minimum plasma drop energy and/or maximum drop size by considering the opaqueness condition Eq. (4) for electron (positron) scattering.

We calculated, as an example, the annihilation relaxation time for an internal plasma drop energy of 0.3–1.2 kJ and radius 3 μm. Because of the relatively low density the annihilation relaxation time is much longer than the pulse duration, which is ≈ 10 fs. We found that in-flight annihilation is fastest at $T = 0.065$ MeV, yet still relatively slow. The radiative positronium production process exceeds the in-flight annihilation at a much lower temperature, 60 eV, leading perhaps to the formation of positronium in the late stages of the drop. If such a low temperature is reached without drastic expansion dilution, very many positroniums can be formed, and positronium formation prolongs the life span of positrons, though the nature of the plasma drop is now different.

The experimental conditions will determine at what temperature and, more importantly for the following argument, rapidity, relative to the laboratory frame of reference, the electron-positron drop will be formed [20,21]. Multipulse arrangements can be easily obtained, resulting in the plasma drop being formed at high rapidity. The greater the rapidity, the greater the effect of the time dilation that prolongs the life span of the plasma drop, as seen in the laboratory. We recognized, in this work, the relative stability against annihilation evaluated in the intrinsic rest frame of the drop. Therefore, it appears possible to create, using high density lasers, a quasistable matter-antimatter plasma drop capable of traveling macroscopic distances before dissipating into a low density cloud of particles.

ACKNOWLEDGMENTS

[1] E. N. Nerush, I. Y. Kostyukov, A. M. Fedotov, N. B. Narozhny, N. V. Elkina, and H. Ruhl, Phys. Rev. Lett. **106**, 035001 (2011); **106**, 109902 (2011).

[2] I. Kuznetsova, D. Habs, and J. Rafelski, Phys. Rev. D **81**, 053007 (2010).

[3] T. Tajima and G. Mourou, Phys. Rev. ST Accel. Beams **5**, 031301 (2002).

[4] R. J. Gold, Astrophys. J. **344**, 232 (1989), Part 1.

[5] J. Letessier, J. Rafelski, and A. Tounsi, Phys. Rev. C **50**, 406 (1994).

[6] T. S. Biro, P. Levai, and B. Muller, Phys. Rev. D **42**, 3078 (1990).

[7] M. B. Kislinger and P. D. Morley, Phys. Rev. D **13**, 2765 (1976).

[8] A. G. Aksenov, R. Ruffini, and G. V. Vereshchagin, Phys. Rev. D **79**, 043008 (2009).

[9] F. Halzen and A. D. Martin, *Quarks and Leptons: An Introductory Course in Modern Particle Physics* (Wiley, New York, 1984), p. 396.

[10] B. L. Combridge, Nucl. Phys. **B151**, 429 (1979).

[11] J. Rafelski and B. Muller, Phys. Rev. Lett. **48**, 1066 (1982).

[12] P. Koch, B. Muller, and J. Rafelski, Z. Phys. A **324**, 453 (1986).

[13] T. Matsui, B. Svetitsky, and L. D. McLerran, Phys. Rev. D **34**, 783 (1986); **37**, 844 (1988).

[14] P. Koch, B. Muller, and J. Rafelski, Phys. Rep. **142**, 167 (1986).

[15] Jean Letessier and Johann Rafelski, *Hadrons and Quark-Gluon Plasma* (Cambridge University Press, Cambridge, England, 2005), ISBN-10: 0521018234.

[16] A. I. Akhiezer and N. P. Merenkov, J. Phys. B **29**, 2135 (1996).

[17] Y. D. Jung, Phys. Plasmas **9**, 4402 (2002).

[18] S. Sen, P. Mandal, and P. K. Mukherjee, Eur. Phys. J. D **62**, 379 (2011).

[19] S. H. Glenzer, H. J. Lee, P. Davis, T. Døppner, R. W. Falcone, C. Fortmann, B. A. Hammel, A. L. Kritcher, O. L. Landen, R. W. Lee, D. H. Munro, R. Redmer, and S. Weber, High Energy Density Phys. **6**, 1 (2010).

[20] L. Labun and J. Rafelski, Phys. Rev. D **84**, 033003 (2011).

[21] L. Labun and J. Rafelski, arXiv:1107.6026.